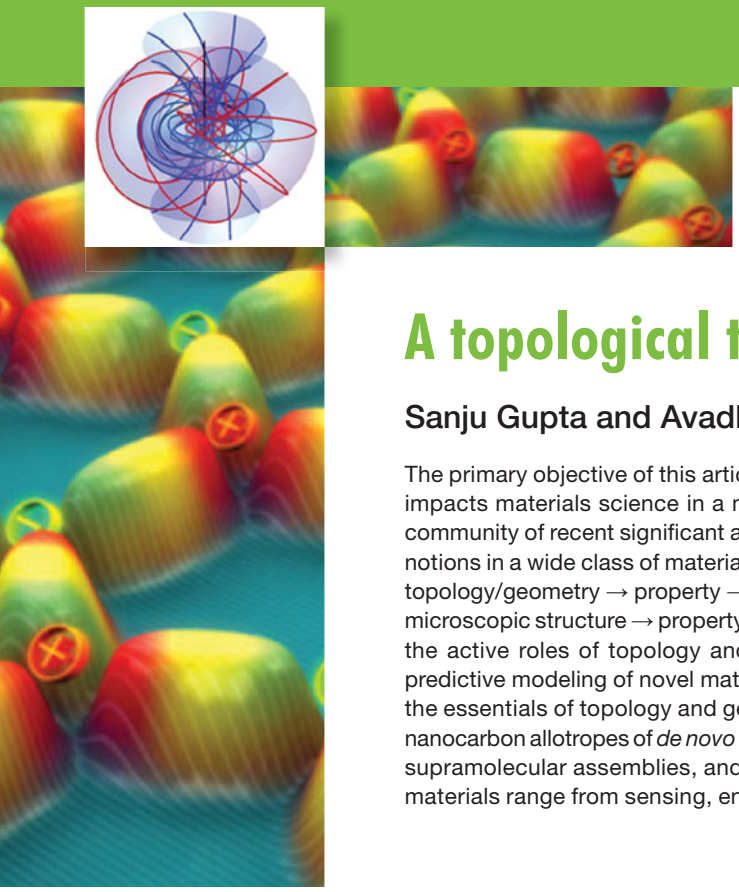


A topological twist on materials science

Sanju Gupta and Avadh Saxena

The primary objective of this article is twofold: to address the key concept of topology that impacts materials science in a major way and to convey the excitement to the materials community of recent significant advances in our understanding of the important topological notions in a wide class of materials with potential technological applications. A paradigm of topology/geometry → property → functionality is emerging that goes beyond the traditional microscopic structure → property → functionality relationship. The new approach delineates the active roles of topology and geometry in design, fabrication, characterization, and predictive modeling of novel materials properties and multifunctionalities. After introducing the essentials of topology and geometry, we elucidate these concepts through a gamut of nanocarbon allotropes of *de novo* carbons, hierarchical self-assembled soft- and biomaterials, supramolecular assemblies, and nanoporous materials. Applications of these topological materials range from sensing, energy storage/conversion, and catalysis to nanomedicine.

Introduction

The notions of topology have been invoked for more than a century in the physical world in fields as diverse as condensed-matter physics, high-energy physics, and cosmology to describe the properties of matter and the universe, respectively, thus spanning the nano- and mesoscales (100 nm–1000 nm) to macroscopic (≥ a few microns) length scales.[1–3] However, topology has not yet taken proper root in materials science with the question: "Do topology and geometry affect materials physical properties at the nano-/mesoscale, and, if so, how can we use them to understand and design materials from this new perspective?" One of the principal goals of this article is to address this and related questions, and materials scientists are now well poised to tap into the richness of this field due to recent advancements in measurements. Thus the goal is to identify and utilize advanced metrological techniques to probe topology and to relate the latter to the functional properties for a broad class of novel functional materials similar to what has been achieved in condensed matter physics.[1] In other words, we look for analogues of identifying "edge states" in quantum Hall materials and topological insulators,[4] which allows us to measure and evaluate transport properties, including surface conductivity, the Hall coefficient, and related parameters.

The topology of a material goes beyond its physical shape and geometry in that it directly affects physical properties such as electronic conduction, charge and spin transport, light transmission, and response to a magnetic field. The nontrivial aspects of topology and geometry have numerous applications in modern condensed matter physics where they play an important role in various physically and technologically interesting systems.[1,4] This incipient appreciation for the importance of topology is beginning to allow researchers to engineer entirely new materials with unusual topologies that lead to either exotic or enhanced properties.[5–7] Nevertheless, for most materials scientists, structural chemists, and biologists, topological methods remain obscure and unusually distant as compared to existing traditional methods.

We first introduce the essentials of topological concepts (for example, handlebars or *genus* of a structure) by means of illustrations without invoking explicit mathematics. We then distinguish between local and global topological aspects of materials and mostly focus on nanocarbons, soft matter, and biomaterials to describe their topology, a variety of topological defects (e.g., vortices, skyrmions),[1,8] and their role in controlling physical properties. To this end, we introduce many topology characterization techniques that underscore the emerging field of topological metrology. The novel and important aspects of this nascent field encompass both qualitative and quantitative trends examined experimentally through measurable quantities such as a change in Raman spectroscopy (RS) bands (e.g., G, D, and 2D) of advanced nanoscale

Sanju Gupta, Western Kentucky University, USA; sanju.gupta@wku.edu
Avadh Saxena, Los Alamos National Laboratory, NM, USA; avadh@lanl.gov
DOI: 10.1557/mrs.2014.28

© 2014 Materials Research Society

https://doi.org/10.1557/mrs.2014.28 Published online by Cambridge University Press

carbons,[9,10] indicative of mechanical loading or deformation, as a function of genus and other topological attributes.

These concepts are also applicable to topological networks[11,12] or nets, periodic structures (e.g., metal–organic frameworks,[13] supramolecular architectures[14]), and geometrical hierarchies found in many soft- and biomaterials.[15] Topological computer algorithms and databases (e.g., TOPOS[16] and EPINET[17]), developed over the past decade and a half in conjunction with advanced visualization techniques, are greatly assisting the design of extended crystalline architectures and frameworks. Beyond the periodic and network structures, we will also discuss the emerging class of topological materials,[18] such as topological insulators[4] and Dirac materials,[19] with an emphasis on the underlying quantum phenomena. Finally, having demonstrated the importance of topology, we hope to establish the topology/geometry → property → functionality paradigm in materials science.

What is topology?

Topology is a field that studies invariance of certain properties under continuous deformation, such as stretching, bending, or twisting, of the underlying geometry. By continuous deformation we mean that nearby points on the object (e.g., a curve or a surface) remain neighbors, and no cutting or gluing is allowed. The continuous change can be continuously reverted, thus retrieving the original shape. We illustrate these apparently abstract concepts through specific examples in **Figure 1** using a pedagogical approach, as explained later.

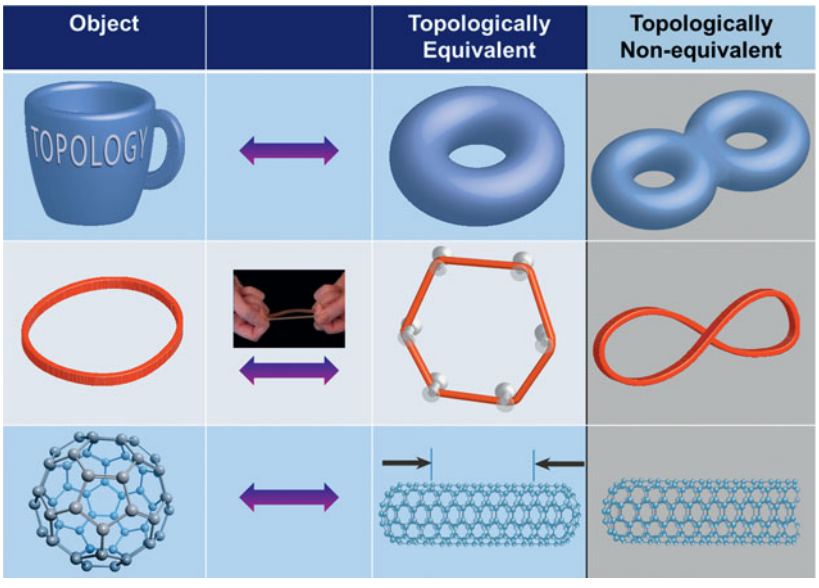


Figure 1. Illustration of topological equivalence between a coffee mug and a donut (top row), between a circle and a hexagon (middle row) (through a stretched rubber band), and between a sphere and a cylinder (bottom row) closed on both sides. The topological inequivalence is delineated in the right column, as a double donut cannot be created by continuously deforming a donut (without cutting or gluing). Similarly, a figure eight cannot be distorted into a circular rubber band without ungluing the intersection point. A one-side open cylinder is topologically different from a closed cylinder because one side has been cut (or unglued).

If we take a rubber band, which is almost a circle, we can continuously deform it to look like a hexagon or other shape. It is topologically equivalent because it is connected by a continuous deformation, stretching in this case. We can undo the deformation (i.e., retrieve the circular rubber band from the hexagon by un-stretching it or removing the push pins, Figure 1). (Note also that circles of different radii are *all* topologically equivalent, by radially stretching them.) Now, assume that the circular object is electrically conducting, such as a metallic ring with a current flowing in it. When it is deformed to the hexagonal shape, the current remains the same. Thus, the current in this case becomes the invariant property that only depends upon the topology but not on the underlying geometry (i.e., insensitive to the shape).

As noted previously, continuous deformation means nearby points remain neighbors, which is true for the circle-to-hexagon deformation and any other polygon (e.g., square or octagon) we could create through stretching the circle. Now consider that the circular rubber band is deformed in a figure-eight shape in which the crossing point is glued. If we unglue this point by stretching, it will become two points, which upon further stretching, will end up as two diametrically opposite points on a circle (i.e., the nearby points do not remain neighbors). Therefore, a circle and a figure eight are topologically inequivalent: a circle has one hole, while a figure eight has two holes, which means they have different topological characteristics, denoted by *genus* (g), where $g = 1$ for the circle and $g = 2$ for the figure eight.

As a two-dimensional (2D) surface example, if we take a coffee mug (made from a deformable soft material, see Figure 1), we can continuously reshape the mug into a donut. The mug handle becomes the hole in the donut. Conversely, we can start with the donut and reshape it into a mug. Thus, a mug and a donut are topologically equivalent since they both have a hole ($g = 1$). A donut, however, is topologically inequivalent to a double donut ($g = 2$) or a simple pretzel because a donut cannot be continuously deformed (without cutting or gluing) into a double donut. Interestingly, a donut is also topologically inequivalent to a cookie, for instance (i.e., no holes, $g = 0$).

Turning our attention now to real-world materials, if we look at the surface of a fullerene (third row, left column of Figure 1), it is the surface of a sphere. Assuming the spherical surface is elastic, if we stretch it laterally, it would appear as a capped nanotube on both sides (i.e., a closed cylinder). Thus, a sphere and a closed cylinder are topologically equivalent, both with no holes ($g = 0$). However, the sphere or the closed cylinder is topologically not equivalent to a one-side open cylinder (third row, right column) because we cannot

https://doi.org/10.1557/mrs.2014.28 Published online by Cambridge University Press

obtain the one-side open cylinder from a sphere or a closed cylinder without cutting it somewhere. In fact, the one-side open cylinder is topologically equivalent to a finite flat disk (or a cookie), as it can be continuously stretched and opened to look like a disk. The open boundary is captured by another topological characteristic, namely the Euler characteristic, χ, besides genus g.

Connecting topology to geometry

Global topology of materials denotes distortion of invariant properties of spaces and objects rather than their topographic (or geometric) description.[1,2] It is characterized by a parameter called genus g (i.e., the "handles" of an arrangement), which is an integer, as mentioned earlier. It is a topological invariant in that it is a conserved quantity under smooth continuous mechanical deformation, and it does not depend on the static or dynamic equations describing the material geometry.[1–3] In other words, if two orientable closed surfaces have the same genus, then they are topologically equivalent. Orientable means that a normal vector is uniquely defined at all points on the surface; the Möbius strip, discussed later, is a notable exception and is a non-orientable surface.[1–3] The genus is related to the Euler characteristic (χ) of a surface, defined by $\chi = 2(1-g)$. However, when there are edges (or boundaries), it can be geometrically expressed as $\chi = V - E + F$, where V, F, and E represent the number of vertices, faces, and edges of a polyhedron "triangulating" the surface, respectively (see **Figure 2**a). The geometry and global topology are intimately connected by the celebrated Gauss–Bonnet theorem: [1,2]

$$\int_S K dS = 2\pi\chi, \qquad (1)$$

where K is the local Gaussian curvature of the closed surface (S) defined later. If we integrate over K on the surface of a given geometry, it equals 2π times the Euler characteristic of that object. Note that K will vary as we deform the surface, or change the geometry, but χ will be unaffected. Regardless of how you may choose to deform the surface (without cutting or gluing), it is uniquely characterized by its topology (χ). Similar to K, χ can be negative. However, the mean curvature H (defined below and see Figures 2b and 2c) and g are strictly non-negative.

To illustrate these concepts, we note that the spherical fullerene (C_{60}) has $\chi = 2$ since $g = 0$ (no holes or handles). All hyperfullerenes ($C_{70,84,90,\ldots}$) and hypofullerenes ($C_{36,50,\ldots}$) are topologically equivalent to a sphere (i.e., $g = 0$, $\chi = 2$). For a simple torus (e.g., a carbon nanoring), $\chi = 0$ since $g = 1$ (see **Table I**). Similarly, for a double torus (or a double nanoring), $\chi = -2$ since $g = 2$. A cylindrical single-walled carbon nanotube (SWCNT) open at both ends is a surface with genus one ($g = 1$) with open boundaries, which implies $\chi = 0$. To understand this, we can draw an edge from one end to the other on the surface of the cylinder (Figure 2a). This would give $F = 1$, $E = 3$, as there are two edges at the ends of the cylinder and $V = 2$; therefore, $\chi = V - E + F = 0$. A carbon nanocone is topologically equivalent to a disk, and thus to a graphene sheet ($g = 0$, $\chi = 2$).

Topology is essentially elastic (or soft) geometry. Geometry is characterized by fixed distances and angles, or more generally on a surface with mean (H) and Gaussian (K) curvatures.[1,10,20] Intuitively, curvature is the amount by which a geometric object (or material) deviates from being flat, or straight in the case of a line. At a given point on a curve, there is one circle of radius R that is tangent to the curve at that point (Figure 2b). The corresponding principal curvature (κ) at that point is simply the reciprocal of the radius (i.e., $\kappa = 1/R$). Analogously, there are two principal curvatures (κ_1, κ_2) at a given point on a surface that measure how the surface bends by different amounts in different directions with respect to that point (Figure 2c). The mean curvature is thus defined by $H = (\kappa_1 + \kappa_2)/2$ and the Gaussian curvature by the product $K = \kappa_1.\kappa_2$. Note that under the resulting condition, $K \le H^2$, a positive K implies that the surface is locally either a peak or a valley, indicating that the surface bends equally on both sides, which is the case for spherical or ellipsoidal geometry. Similarly, hyperbolic geometry has a negative K,[1,10,20] which means that the two principal curvatures have different signs (e.g., a hyperboloid [a hyperbola rotated around its axis]), or the surface locally has saddle points. $K = 0$ implies that the surface is flat in at least one direction (e.g., a plane, cylinder, or cone). Surfaces with $H = 0$ are called minimal surfaces; some examples include a plane (trivial), a helicoid, a catenoid, and periodic negatively curved carbon (Schwarzite).[20] Next, we demonstrate and discuss nanocarbon allotropes as a prominent example of topological variation in greater detail.

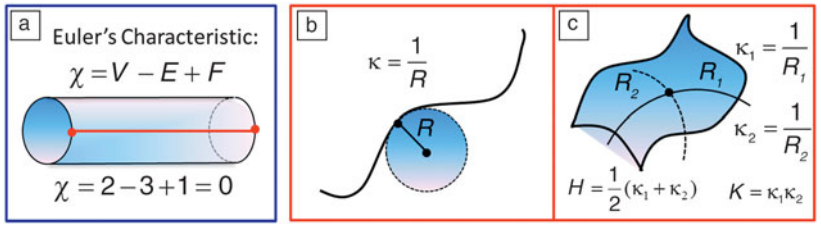


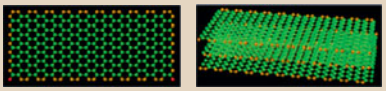
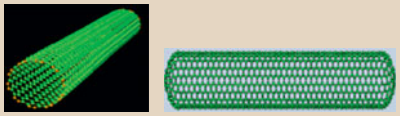
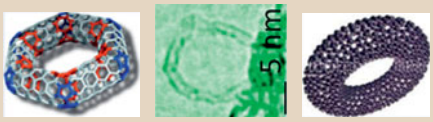
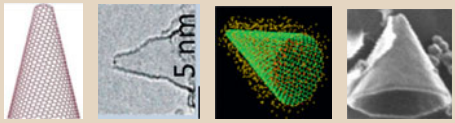
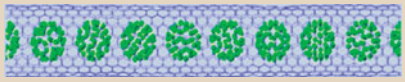
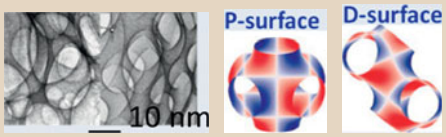
Figure 2. (a) Euler characteristic (χ) for surfaces with open boundaries. The red line ending on the circular boundaries creates two vertices ($V = 2$). (b) Principal curvature of a curve (κ) at a given point is the inverse of the radius (R) of the tangent circle. (c) A surface has two principal curvatures (κ_1, κ_2) defined by the radius of two orthogonal tangent circles (R_1, R_2) at a given point, defining geometric mean (H) and Gaussian (K) curvatures. Note: E, number of edges; F, number of faces; κ_1, principal curvature for tangent circle 1; κ_2, principal curvature for tangent circle 2.

Topological taxonomy of nanocarbons

Nanocarbons exist in numerous geometries and topologies that range from planar or monolayer

https://doi.org/10.1557/mrs.2014.28 Published online by Cambridge University Press

Table I. Topology of nanocarbon allotropes.

Geometry	Schematic	Topological Characteristics	
		g (Genus)	χ (Euler)
Positive Gaussian Curvature			
Mono-and multi-layered graphene (HOPG)		0	2
Fullerenes and hyper-/hypo-fullerenes		0	2
Single-walled carbon nanotube (SWCNT); open (closed)		1 (0)	0 (2)
Nanoring/nanohoop		1	0
Nanohorn/nanocone		0	2
Double-(DWCNT), oligo-(OWCNT) and multi-walled carbon nanotubes (MWCNTs)		Complex Geometries	
Peapod			
Negative Gaussian Curvature		*g* (Genus) unit cell	χ (Euler)
Negatively curved carbons/ Schwarzites (3D)		3	–8
Graphene/carbon nano-ribbon (G/CNR)/helicoidal (2D)		0	1

Topological characteristics of distinct nanostructured curved carbons with different genus (*g*) and Euler characteristic (χ). Note that both positive and negative curvature geometries are depicted. Note: HOPG, highly oriented pyrolytic graphite; P-surface, primitive Schwarz surface; D-surface, diamond Schwarz surface; *c*, helicoid pitch.

and multilayer graphene (the youngest member in the family of synthetic nanocarbons),[21] nanotubes (single-, double-, oligo-, and multi-walled), fullerenes and their analogues (hypo- and hyperfullerenes, the oldest member in the synthetic nanocarbons, which marked a pivotal moment in the field of nanotechnology),[22,23] to nanorings, nanocones, nanohorns, and peapods, which we collectively refer to as topologically distinct geometric allotropes of carbon.[9] These synthetic nanoscale carbon allotropes represent a growing family of fascinating and aesthetically pleasing architectures with outstanding material properties. In addition, while carbon remains the element of choice for applications, its allotropes offer multifunctional behavior and provide a fertile playing field for expounding the nontrivial notions of global topology

https://doi.org/10.1557/mrs.2014.28 Published online by Cambridge University Press

and unusual geometric attributes (see Table I).[10,20] These concepts are applicable beyond the nanoscale, to the mesoscale, and all the way to the very shape and structure of the macroscale universe. Some of the fullerenes and related nanoscale carbons are known to have formed extraterrestrially in interstellar space, meteorites, lunar rocks, and terrestrial sediments.[22]

Multiwall carbon nanotubes and fullerenes ("nano-onions") possess complex topologies, as do peapods. The latter comprise SWCNTs filled with C_{60} fullerenes. Similarly, X-, Y-, and T-junction shaped nanotubes also have complex topologies.[9] Assuming closed boundaries, Y- and T-junctions have $g = 2$, $\chi = -2$, whereas the X-junction has $g = 3$, $\chi = -4$. Among the negative Gaussian curvature ($K < 0$) periodic carbon allotropes, Schwarzite has a complex topology with $g = 3$, $\chi = -8$ per unit cell (Table I).[20] Similarly, a helicoid-shaped graphene nanoribbon would have $g = 0$, $\chi = 1$.[20]

We summarize the global topology of nanocarbons in Table I in terms of g and χ. Note that the nanocones, nanodisks, and nanotubes closed at one end are topologically equivalent to the flat graphene sheet ($g = 0$). Similarly, fullerenes (C_{60}), hyperfullerenes ($C_{70,84,90,\ldots}$), hypofullerenes ($C_{36,50,\ldots}$), and capped nanotubes have the topology of a sphere ($g = 0$). As noted, due to the boundaries captured by χ, open nanotubes have a different topology ($g = 1$, $\chi = 0$) than those of closed ones ($g = 0$, $\chi = 2$). Carbon nanotori and nanorings are topologically equivalent to a torus ($g = 1$, $\chi = 0$).

Stable π-conjugated aromatic Möbius annulenes and Möbius strips of single crystals of certain charge-density wave trichalcogenides have been recently synthesized.[24] The unusual spin and electronic properties of graphene Möbius strips have also been explored.[25] The Möbius strip is a structure with an indistinguishable inner and outer surface—a non-orientable surface[1–3] with Euler characteristic $\chi = 2 - k = 0$, where $k = 2$ is its non-orientable genus (different from the usual or orientable genus). Multiple twists of the graphene nanoribbons result in topologically distinct strips as observed in transmission electron microscopy (TEM) images.[26] A typical twisted graphene nanoribbon has $g = 0$ and $\chi = 2$. These concepts are applicable to a much broader class of materials discussed next.

Topology of soft/biomaterials and complex networks

Analogous to carbon nanomaterials, other hard-, soft-, and biomaterials come in a variety of topological forms. Some examples include titania (TiO_2) and silica (SiO_2) nanotubes,[27] boron-nitride nanotubes and nanotori,[28] helical gold nanotubes,[29] Möbius conjugated organic materials,[24,30] mesoporous silica networks,[12] di- and tri-block copolymers,[31] micelles, colloids, micro-emulsions, biological vesicles,[32,33] microtubules, folded proteins, knotted DNA, supramolecular structures, and photochemistry in restricted space.[14] The topology of mixed di- or triblock copolymers,[31] as well as single and double gyroid structures[15] (in butterfly wings and bioinspired photonic bandgap materials), zeolites, and other metallo–organic frameworks[13] (MOFs) belongs to periodic minimal surfaces.[20,34–36] Also, foams,[37] for instance, possess an interesting network topology, and they change configurations at the local level via a T1 switch (see **Table II**), in which the interface between two bubbles shrinks to zero length and then expands to a finite length in another direction, thus causing a local topology change.[38] In addition, many biological processes, including DNA and RNA structure and protein folding, involve network, braid, and knot topologies.[39]

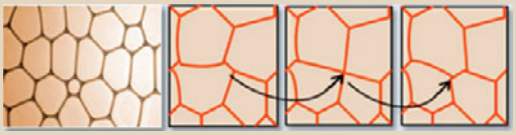
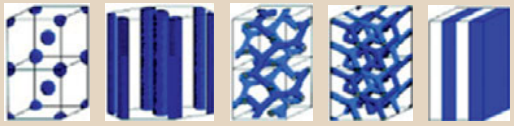
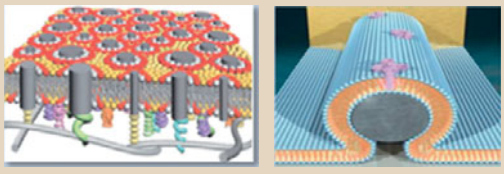
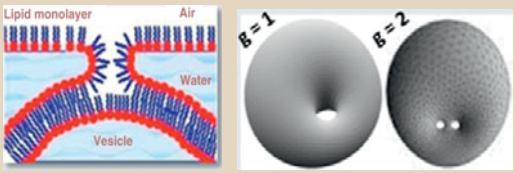
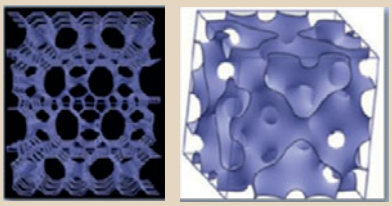
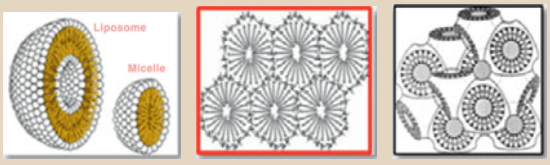
A network has connected nodes and lines in various ways.[11,12] Lattices are a special kind of network in which the lengths are the same in each periodically repeated unit, called a unit cell. Two networks may have different distances between nodes and other characteristics and yet may have identical topologies (i.e., they can be continuously deformed into each other). As a special case, a square lattice is topologically equivalent to an oblique lattice but not to a triangular lattice. Protein interaction networks,[11] biochemical metabolic networks,[40] polymer networks,[41] and mesoporous materials[12] are examples in which correlations between the network structure (or topology) and functional properties provide useful insights into design strategies. Similarly, for studying 2D and 3D microstructure evolution in the context of crystal grain growth[42] and topological optimization of materials microstructure[43] (as well as of multicellular structures such as foams, bubbles, and biological tissues), network topology provides an efficient tool.[44] Specifically, grain growth strongly favors particular grain topologies.[42]

In soft- and bio-matter such as di- and tri-block copolymers[31] and photonic crystals (in butterfly wings as well as in weevil chitin[15]), depending on the relative concentration of the two constituents and temperature, the topology can change from a lamellar structure to a tubular structure or to a gyroid structure.[15,31,45] These can be classified as a phase change characterized by a change in topology. Some materials are unable to reach their minimum energy state due to topological reasons resulting in topological frustration.[46] This is very common during protein folding, but graphene nanoflakes can also exhibit this phenomenon[47] where magnetic order can develop as a consequence.

Table II also shows examples of complex topology in liquid crystals and block co-polymers. The second row shows multiple dislocations in a liquid crystal[48] (left panel) and a stacking of cylindrical structures in a hexagonal lattice, with each cylinder possessing a complex topology (i.e., a bundle of helicoidal layers).[49] The self-assembly of di- and tri-block polymers results in a variety of complex topologies (third row) as a function of the relative concentration of different types of polymer blocks and the interaction energy between different types of monomers[31] (i.e., the Flory-Huggins parameter). Some depicted examples include lamellar, cylindrical, globular, gyroid, and double gyroid structure. Interestingly, the gyroid is a triply periodic minimal surface (mean curvature $H = 0$) that belongs to the family of P and D (primitive and diamond) Schwarz surfaces[34–36] and separates space into two identical

https://doi.org/10.1557/mrs.2014.28 Published online by Cambridge University Press

Table II. Topology of soap bubbles and foam, liquid crystals, di- and triblock copolymers, biomembranes, vesicles, zeolites, metallo–organic frameworks, and supramolecular assemblies.

Geometry	Schematic	Topological Characteristics		Suggested Metrology
		g (Genus)	χ (Euler)	
Soap bubbles and foam		Network topology		Optical imaging [38]
Liquid crystals (double-dislocation)		Complex topology		Non-linear optical fluorescence microscopy, laser lithography[91,92,93]
Di- and tri-block co-polymers (lamellar)		Complex topology		Small-angle x-ray and neutron scattering (SAXS/SANS)[45]
Bio-membranes (lamellar)		0	2	Optical fluorescence microscopy and SAXS/SANS[51,52]
Vesicles (w/ and w/o holes)		0/1,1,2	2/0,0,–2	Optical fluorescence imaging[33]
Zeolites (micro-/mesoporous, metallo-organic frameworks [MOFs])		3	–8	HRTEM, SAXS/SANS, and x-ray tomography[34,35,78,79]
Supramolecular assemblies		1	0	Optical fluorescence imaging and SAXS/SANS[51,52]

The foam network rearranges itself through T1 switching events shown by black arrows, which are local topological changes as depicted in the side panel (first row). The MOFs (sixth row) are a periodic minimal surface with negative Gaussian curvature and $g = 3$, $\chi = -8$ per unit cell. Corresponding suggested metrologies for probing topology/geometry are also listed. Note: SAXS, small-angle x-ray scattering; SANS, small-angle neutron scattering.

labyrinths of passages. This peculiar structure was discovered in 1970 by Alan Schoen (then a scientist at NASA).[50] It also corresponds to the last space group (number 230, Ia $\overline{3}$ d).

Biomembranes can be flat (lamellar) or curved depending on the structures they enclose (fourth row),[51] and they can also morph into a spherical or toroidal topology, in some cases with $g > 1$ (fifth row). As indicated previously, MOFs[13] also form periodic minimal surfaces and gyroid-like structures (sixth row). Finally, supramolecular assemblies may emerge with a variety of topologies, including spheroidal, periodic with $g = 1$, or even a gyroid-like structure.[52] It is highly desirable to probe and quantify the topological attributes of the examples portrayed in Tables I and II.

https://doi.org/10.1557/mrs.2014.28 Published online by Cambridge University Press

Probing topology of nanocarbons and metrology

Probing topological effects on physical properties of materials in a significant way and identifying topological metrics through analytical techniques that relate to one (or more) experimental physical quantities are some of the pressing questions for materials scientists. As a first step in this direction, we recently attempted to describe the differences between various nanoscale carbons and provided a semi-quantitative topology assessment via monitoring characteristic lattice phonon modes, measured using resonance RS in the first- and second-order, thereby capturing the electronic spectra and elucidating a viable approach.[9,10] While the latter can also be obtained using traditional UV-visible optical spectroscopy, high-resolution transmission electron microscopy provided the much needed nanoscopic microstructures of various carbons. Understanding these geometric allotropes of nanocarbons, particularly in terms of their topological characteristics, becomes indispensable because it goes well beyond the traditional paradigm of microscopic structure → property → function correlation to the global topology/geometry → property → function relationship. From this perspective, we can elucidate the notion of global topology and curvature for a range of technologically important nanoscale carbons, including tubular (SWCNTs), spherical (hyperfullerenes), toroidal (nanorings), and conical/complex (nanocones, nanohorns) geometries.

Various forms of carbon at all spatial lengths undoubtedly play a pivotal role for topology due to their structural diversity and geometries from a curvature and topology perspective, thus uniquely positioning carbon as a fertile playing field for global topology versus geometry and curvature attributes. Based on extensive studies on graphite, an infinite multilayered graphene structure with primarily sp^2-bonded carbon (sp^2 C) hybridization, it becomes apparent that graphene is the 2D building block for carbon allotropes of every other dimensionality.

Raman spectroscopy technique

RS has emerged inarguably and historically as one of the potential analytical tools and an integral aspect of structural characterization of graphite and related carbon materials at the nanoscale, revealing not only the collective atomic/molecular motions but also localized lattice vibrations.[53,54] Some of the primary reasons for this advantage are the strong Raman response to the π-states in sp^2 C systems due to resonance enhancement (resonance Raman spectroscopy [RRS]); its simplicity for high-symmetry nanotubes and fullerene species, facile access, and noninvasive nature; and its ability to provide invaluable information on elementary excitations (phonons, defects, stacking order/disorder) in graphite as well as the number and orientation of graphene layers, the quality and type of edges in graphene, effects of perturbations (electric and magnetic fields, strain, doping, disorder, and functional groups), and finite size of the crystallites parallel and perpendicular to the hexagonal axis of the probed material. These advantages result from the sensitivity of RS to the changes that occur in the atomic structure arising from multiple causes.

Our motivation here is at least twofold: (1) to amplify on the structures observed in high-resolution electron microscopy and RRS studies of various nanoscale carbons with arbitrarily low genus by monitoring and identifying the effects in vibrational modes (usually ignored) arising due to curvature, and (2) to provide Raman spectra for otherwise unexplored nanoscale carbons to identify a truly topological metric.[9,10] In doing so, we aim to gain a deeper insight and develop a unified understanding from the global topological and curvature perspectives by monitoring the shift in wavenumbers of prominent Raman bands of diverse curved nanocarbons as a topological indicator/metric. In addition, it is anticipated that these shifts in wavenumbers are translated into changes in local curvature resulting from local topological defects, namely either the pentagon-heptagon (P-H) or Stone-Wales (S-W) pair defects and/or the mitosis defect,[55–60] as well as into boundary conditions that are applicable in theory while calculating optical absorption and vibrational spectra using tight-binding models that help map the electronic structure of these nanomaterials.

Resonance Raman spectra were measured using a commercial micro-Raman spectrometer equipped with a 2400-g/mm grating, ion-etched Super-Notch-Plus filter, an argon-ion laser operating at excitation wavelength λ_L = 514 nm (laser incident energy E_L = 2.41 eV), and a power <10 mW to avoid local heating and thermal degradation (spectral resolution of ~1 cm^{-1}, and Spectra Max software for Windows to accumulate raw data). Raman spectra were recorded in the wave-number range of 1000–3000 cm^{-1} in backscattered configuration and analyzed.[9] We measured resonance micro-Raman spectra of pristine monolayer graphene (and equivalently an infinitely multilayered graphene or highly oriented pyrolytic graphite, HOPG), a hyperfullerene (C_{84}), an open-ended SWCNT, a single-walled nanoring (SWNR), a single-walled nanohorn (SWNH), and a nanocone both in the first- and second-order spectral regions (**Figure 3**a–b). Some of these carbon forms were produced in very small quantities using either the electron beam irradiation of SWCNT[61] or other processing techniques, such as thermal annealing of ultradispersed diamond.[62] Because all of these materials are sp^2 C derivatives, it is instructive to compare their Raman spectral features with planar HOPG and monolayer graphene.

Prominent bands of interest in the first-order Raman spectra for all of the nanocarbons are D and G bands occurring at ~1340 cm^{-1} and ~1580 cm^{-1}, respectively. The higher wavenumber G band is associated with the tangential C-C stretch or the tangential displacement mode having an E_{2g} symmetry. For plasma-enhanced chemical vapor deposited SWCNT, the G peak decomposes into two main peaks around 1562 cm^{-1} and 1593 cm^{-1} (G^+ and G, respectively) with a shoulder at ~1550 cm^{-1} (G^-). These features have previously been assigned to the E_{2g} symmetry mode of graphite that results from the splitting of an intralayer stretching mode. This splitting arises due to the curvature-induced re-hybridization of σ*-π* states.[54,63] In fact, this re-hybridization strengthens the C–C bond, which

https://doi.org/10.1557/mrs.2014.28 Published online by Cambridge University Press

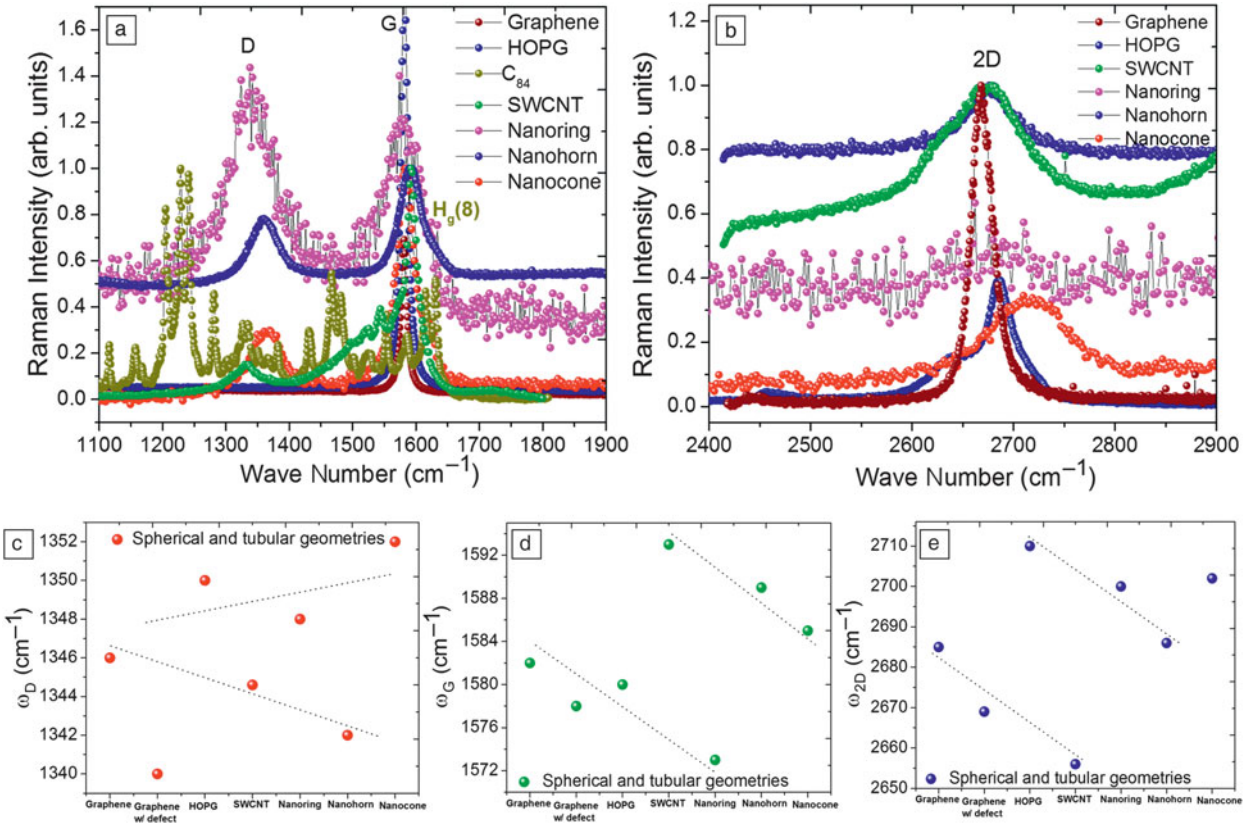


Figure 3. Experimental (a) first-order and (b) second-order resonance Raman spectra for monolayer graphene with or without defects, infinite multilayered graphene, or highly oriented pyrolytic graphite (HOPG), hyperfullerene C_{84}, single-walled carbon nanotube (SWCNT), single-walled nanoring and nanohorn, and tip of the nanocone showing prominent bands of interest, namely D, G, and 2D, and $H_g(8)$ for C_{84}. The Raman intensity is normalized with respect to the higher intensity G band. (c–e) show variations in the Raman frequencies ω_D, ω_G, and ω_{2D} for D, G, and 2D bands, respectively. Since the Raman bands assignment for C_{84} is different, the variation is not shown for C_{84} and is mentioned in the text wherever appropriate. The dotted lines in (c–e) are drawn to guide the eye.

yields relatively high elastic constants for the SWCNTs. It is worth mentioning that the excitation wavelength of 514.5 nm (or photon energy of $E_L = 2.41$ eV) preferentially excites semiconducting SWCNTs (mean diameter of $d_t \sim 1.3$ nm) and is in resonance with the E_{22}^{SS} branch of SWCNT 1D density of states. Qualitatively, the Raman modes of SWCNTs seem to be narrow and sharp, indicating high uniformity and a low level of impurities, thus of reasonably good crystalline quality.[61]

Variation in prominent Raman bands

The D band in sp^2 C materials is the disorder-activated band with A_{1g} symmetry in the first-order scattering process arising from in-plane substitutional heteroatoms, vacancies, grain boundaries, or other defects and finite size effects, all of which lower the translational symmetry in a quasi-infinite lattice and violate momentum conservation. Therefore, association of the D band with symmetry-breaking phenomena results in a band intensity that is proportional to the phonon density of states, which is applicable to practically all of the sp^2 C-based material systems. Note the onset of the D band in Figure 3, which is absent for defect-free HOPG and graphene.[60,64]

Stable sp^2 C spherical cages are the most abundant fullerenes (C_{60}) with somewhat lower yields of higher analogues such as C_{84}. Figure 3a shows the effect of curvature and geometry on the experimentally observed specific Raman mode in the high wave-number regime for spheroids (D_{2d}–C_{84}) compared with HOPG. They are synthesized and isolated following Reference 65. While there are only a few Raman lines for C_{60}, the spectrum for C_{84} shows many more lines due to a deviation from the spherical geometry (usually oblate), large number of C atoms, hybridization, and also to a more reduced symmetry than that of the icosahedral symmetry I_h for C_{60}. While it is difficult to interpret the Raman spectrum for C_{84}, a strong vibrational structure resembling a downshifted and split C_{60} spectrum is apparent for C_{84}, where the center of gravity of the two Raman bands is shifted by a factor of ~0.85 and 0.87 with respect to the $A_g(2)$ (a well-known pentagonal pinch mode for C_{60} occurring at ~1470 cm^{-1}) and $H_g(8)$ bands at ~1575 cm^{-1}, respectively. A correlation between the cage mass and the frequencies from fullerene modes of similar origin thus seems to be justified.[66,67]

Figure 3a also shows the Raman spectra for a SWNR, a SWNH, and a nanocone. SWNHs were obtained from Sano's

https://doi.org/10.1557/mrs.2014.28 Published online by Cambridge University Press

and Yudasaka's groups in Japan, both exhibiting similar phonon spectra.[68,69] They were grown by a DC electric arc discharge between two graphite electrodes submerged in liquid nitrogen. The internal structure of SWNH is described as a mixture of "dahlia-like" and "bud-like" structures as observed by TEM. SWNHs have a graphitic carbon structure similar to that of the usual carbon nanotubes except that they are twisted. One of the potential applications of SWNHs is in fuel cell electrodes because of their large surface area and easy gas and liquid permeation.[70] On the other hand, SWNRs ($g = 1$) were formed by electron-beam irradiation.[61] The Raman spectra of SWNH and SWNR show typical nanocarbon disorder D (~1350 cm^{-1}) and G (~1580 cm^{-1}) peaks (Figure 3a). The SWNR Raman spectrum resembles that of SWCNT, but it differs somewhat, accounted for by the shift of the G band. Alternatively, the G band is upshifted, leading to graphene planes with compressive microscopic strain attributed to the graphene plane curvature. This curvature is invoked to explain the relaxation of the Raman selection rules and the appearance of new, albeit weak, Raman peaks at 1100 cm^{-1} and 1740 cm^{-1}.

Nanocone tip Raman data were obtained from Gogotsi's group and analyzed.[71] While the D peak shifts from its average position at ~1340 cm^{-1}, the G peak shifts from 1580 cm^{-1} for HOPG to ~1585 cm^{-1} for a synthetic carbon nanocone. The upshift of the Raman band was attributed to the simultaneous presence of the curved cone surface and smaller crystallite size giving rise to phonon confinement in the nanocone. The presence of a D band in all phonon spectra indicates that the surfaces of cones and graphite with micron-sized crystallites or domains were not perfectly wrapped by graphene. A qualitative observation of the broadening of the G band results from the conical wrapping of layers and bonding of graphene sheets. From the subtracted Raman spectra for a cone and HOPG, it is clear that the Raman spectrum for nanocones is composed of at least two contributions: microcrystalline graphite subsurface carbon layers and multiwall or graphite whiskers close to the surface.

Raman bands of the representative materials mentioned previously were quantitatively analyzed in terms of the position of D and G bands as a possible topological metric due to their sensitivity toward structural modification, however, with weaker or "group" trends. Figure 3c–d summarizes the main effects, including those of graphene and HOPG. Generally speaking, the presence of the G band is a direct indication of the presence of a sp^2 C network, and the shift (either decrease or increase) in the highest wave number position is a measure of (a) different sp^2 C configurations; (b) curvature-induced re-hybridization and probably a mixed hybridized character; (c) compressive or tensile stress/strain; and (d) possible phonon confinement (or vibrational localization). It seems that the tensile strain in graphene planes induces curvature by the introduction of pentagons in the hexagonal network governed by Euler's theorem for fullerenes.[9] While the Raman bands for the nanocone and nanohorn appear at almost similar positions, the nanoring lies in the category of a different geometry. (Ideally, the nanoring is a toroidal geometry with genus one.) A quantitative understanding of the Raman line shape and wavenumber shift due to the geometry and topology in these carbon nanostructures requires properly accounting for the changes in both phonon and electronic density of states and the concomitant modification of the electron–phonon interaction. Indeed, recent theoretical studies on nanotori, nanocones, and nanohorns have provided valuable insights in this direction, in direct concurrence with our limited findings.[72,73]

While the first-order Raman spectra features furnish information about the energies of elementary excitations in solids at the center of the Brillouin zone (BZ), the second-order Raman spectra provides information about the dispersion relations of phonons or high symmetry points of the BZ, which in some respects is the information that optical absorption spectroscopy yields on the electronic band structure. Moreover, in the Raman spectra from low-dimensional (1D and 0D) systems, higher-order or overtone modes are equally or sometimes more informative for phonon spectral representation than for 3D solids or bulk systems. This is related to the fact that in 3D solids, the inclusion of two or more phonon modes in a scattering process relaxes the wave vector selection rule and therefore gives a relatively broad structure to the Raman spectra. However, in low-dimensional materials, the (momentum) k-space integration is only in one direction, and the 2D band (sometimes it is also denoted as D* in the literature) is symmetry allowed by momentum conservation; therefore, the overtone Raman features remain relatively sharp and are an intrinsic feature. The 2D band in the Raman spectra of most of the sp^2 C materials is generally more intense than that of its first-order counterpart and has almost the same intensity as the G band. In general, almost all of the data are consistent with the frequency relation $\omega_{2D} \cong 2\omega_D$, particularly for the nanotubes.

As for the physical origin of the disorder-induced D band, it was interpreted initially in terms of phonon density of states maxima, but this was revisited by Vidano et al.,[74] who showed that the D band is dispersive (i.e., the D band changes with incident laser energy, E_L). The position of the D band upshifts with increasing E_L in a linear way over a wide range, the slope ($\Delta\omega_D/\Delta E_L$) being about 50 cm^{-1}/eV independent of almost any type of sp^2 C bonding. Likewise, the 2D band also exhibits dispersive behavior, with the slope being twice that for the D band (i.e., 100 cm^{-1}/eV). Baranov et al.[75] made the first successful attempt to explain the origin and the dispersive behavior in wave numbers of D and 2D bands, namely double resonance, and Thomsen and Reich[76] further developed this. Figure 3b shows the second-order Raman spectra of all the representative nanocarbons discussed earlier. Each of the Raman spectrum intensity is normalized with that of the G band. Given the dispersion with laser energy, the "dispersive behavior," albeit with curvature, in these nanoscale carbonaceous materials both in the D and 2D bands, is shown in Figure 3c and 3e, respectively, which is akin to Figure 3d for the G band. Electronic structure is usually captured through resonance Raman spectral features, as well as through the differential second-order

https://doi.org/10.1557/mrs.2014.28 Published online by Cambridge University Press

Raman spectra, wherein the observed spectra are interpreted in terms of maxima in the joint electron density of states. The "dispersion" in the position of D and 2D bands is the key factor in the quantitative evaluation of geometrical curvature and corresponding topology, assigned to either microscopic tensile or compressive stresses/strains depending on down- and upshifts, respectively.

Alternatively, these bands are also useful for quantifying mechanical deformation in nanocarbons alone or when combined with host materials forming functional nanocomposites. While the G band variation is rather weak, the variation in D and 2D bands provides yet another measure of the curvature/topology, as they are sensitive to structural modification induced by local pentagons or intrinsic defects. Following the "isolated pentagon rule," two adjacent pentagons (mitosis defect)[59] are somewhat unstable, which manifest curvature, thus introducing microscopic stress fields in the C–C bonding network. Since the introduction of pentagons in an otherwise hexagonal carbon system modifies the electronic structure, all the properties dependent on the electronic structure of carbon are affected. Moreover, it turns out that the ordering of the valence or highest occupied molecular orbitals states is largely unaffected by the curvature, only the lowest unoccupied molecular orbitals states are affected. Besides, theoretical numerical calculations for nanotubes show smoothening of the van Hove singularities in density of states devoid of standard singular behavior, with an increasing number of layers and an increasing curvature or strain. This can be explained by an increase in the "mass factor" due to geometry/curvature, which lowers the wave number in the phonon spectra. The obtained RS results are in qualitative agreement with the tight-binding calculations for the closed nanotube.[77] Similar information for the hyperfullerenes is not shown because the assignment of bands differs from that for other sp^2 C materials discussed. Once established, this knowledge provides a powerful machinery to understand newer nanocarbons and indeed points to an unprecedented emergent paradigm of global topology/curvature → property → functionality relationship.

Other metrological techniques

We emphasize that these concepts are applicable to other topologically distinct nanomaterials, which include boron-nitride (BN) nanotubes and nanotori,[28] helical gold nanotubes,[29] and Möbius conjugated organics.[24,30] In addition to RS, there are other techniques such as small-angle x-ray and neutron scattering (SAXS/SANS), scanning electron microscopy, TEM, and various optical imaging techniques that can be used as metrological tools to link materials topology. Topological correlations that could be obtained via scattering techniques would be highly desirable in this regard. Similarly, two-point ($\mathbf{r}$ and $\mathbf{r}'$) network topology correlations could be obtained by appropriately choosing the momentum k range in scattering experiments. X-ray tomography has also been used for the topological characterization of porous media and porous networks.[78,79] Eventually, metrological techniques will allow us to probe topology from nano- to meso- and macroscale lengths in various materials.

Topological defects: Local versus extended

Local or extended deviations from the given topology of a material result in topological defects. They can substantially alter materials properties or give rise to entirely new functionality in some cases. In the case of carbon defects, local violation by topological defects (i.e., violating nanoscale translational order inherent in periodic nanostructures) leads to novel curved nanocarbons,[9] which in turn transcends to the global topology of the material. In particular, a pentagon (or a heptagon) is a local topological defect in the hexagonal network of graphene or graphite, or a defect with sp^3 character in a sp^2-bonded lattice. Presence of these defects not only introduces curvature in the material, thus affecting the global topology, but also affects the electronic structure, physical properties, and functionality. It has been recently reported that even with defects, graphene is the strongest material, and "so strong that it would take an elephant, balanced on a pencil, to break through a sheet of graphene the thickness of Saran Wrap."[80] In other materials, for instance, connectivity at various nodes in cross-linked polymer networks[31,41] and silica networks[44] defines the local topology, which is characterized by local clusters, bond-angle distributions, and radial correlations.

Materials properties crucially depend on the presence and type of defects in the lattice. In the same vein, topological defects are even more interesting, as their existence puts a novel twist on the properties of materials. In particular, it is the mesoscale control and characterization of these defects that will allow us to tap into the full potential of topology in materials. Semiconductors are a good example in which a ppm or ppb level defect concentration can alter the transport properties rather substantially. Vacancies, substitutional, interstitial, and other point defects are examples of non-topological defects. Extended defects such as dislocations, disclinations, domain walls (including twin boundaries that connect two different crystallographic orientations or variants), vortices, and magnetic flux tubes in Type II superconductors are all examples of topological defects.[1] Topological defects occur either at the boundary of two equal energy states, such as the interface between two different magnetic moment directions or two different crystalline orientations, or when the crystalline continuity is broken, for instance, in a screw dislocation. Such defects are responsible for many common phase transitions, including melting and certain magnetic transitions. Topological defects are characterized by, in addition to the material's genus and Euler characteristic, their topological charge (e.g., the Burgers vector strength can be viewed[81] as "topological elastic charge density").

Familiar defects in materials include domain walls between two differently oriented crystals or magnetic states, which are in fact a kind of topological defect called solitons. Solitons are ubiquitous in nature as well as in materials; they are created by a cancellation of the nonlinear and dispersive effects in

https://doi.org/10.1557/mrs.2014.28 Published online by Cambridge University Press

the material (or medium).[82] Dispersive refers to the speed of a soliton or solitary wave that depends on its frequency. Ideally, solitons (and domain walls) propagate through a material or medium or through each other without altering their shape. Similarly, some superconducting materials and Heisenberg magnets exhibit other types of topological defects (e.g., vortex lines and a variety [spiral, helical] of spin textures as well as flux tubes). Missing half planes in crystals are also extended topological defects denoted as edge dislocations. Likewise, fivefold coordinated entities in some crystals are actually orientational disclinations (i.e., topological defects in an otherwise sixfold coordinated triangular lattice).

Here, we choose to describe more elaborate topological defects because they have been observed in many complex functional materials and possess rich internal structures, which affect materials properties in unexpected, multiple ways. **Figure 4** depicts a half dozen such exotic topological defects in a diverse variety of functional materials. Skyrmions (Figure 4a) are spin textures that cover a sphere once (i.e., spin orientation goes from 0 to π) and have been observed in both metallic and insulating chiral magnets.[8,83] Unlike vortices, skyrmions do not have a core and thus can be driven by a small electrical current with apparent applications in information storage. However, similar to vortices, they also form a periodic structure called the skyrmion lattice, which has been observed in chiral magnetic metals,[8] chiral magnetic insulators (and multiferroics),[83] and chiral nematic liquid crystals.[84] Isolated magnetic monopoles (or magnetic charges) are otherwise deemed impossible to exist, but they have been recently observed in artificial spin ice[85] (Figure 4b), which is an example of a frustrated magnet with application in memory devices. The skyrmion lattice can also exhibit magnetic monopoles (and associated Dirac strings).[86]

The middle row in Figure 4 shows other exotic topological defects. Figure 4c depicts 3D boojums with a complex structure for colloidal particles dispersed in a liquid crystal.[87] Boojums are surface defects, first observed in superfluids (with hedgehog point defects being their bulk counterpart), and are now ubiquitous in soft materials, including Langmuir monolayers, liquid crystals, and even in Bose–Einstein condensates. Figure 4d depicts a Schlieren texture[48,88,89] related to the "director field" of a uniaxial nematic crystal observed under a polarizing microscope. Some nanoscale ferroelectrics and multiferroic thin films can show double (electric and magnetic) vortices,[90] as depicted in Figure 4e, which can affect the magnetoelectric response of the material. Finally, Figure 4f shows a pentagon-heptagon pair topological defect in a carbon nanotube,[57] which renders it with a curvature. Other unusual topological defects in materials (e.g., umbilical defects[89]) have not been discussed here.

From a metrological perspective, another recently observed exotic topological defect is the Hopf fibration in a chiral nematic liquid crystal.[91] The Hopf fibration is a complex texture that resembles a series of linked rings wrapped around a torus (see **Figure 5**a, left column). It can be controllably generated experimentally in cholesteric liquid crystals (i.e., nematics) with a twist (or preferential handedness), as depicted in Figure 5b with a specific color coding. Using specially shaped laser and electron beams, one can orient the molecules in a liquid crystal to form not just vortices and knots, but also exotic topological

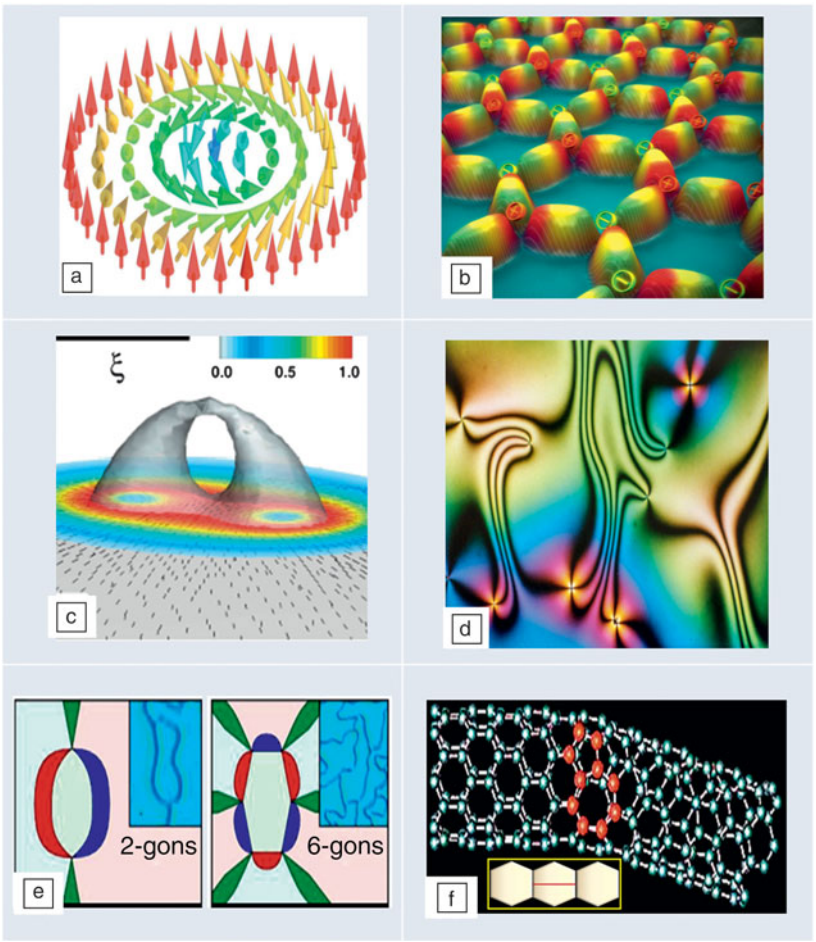


Figure 4. Exotic topological defects in functional materials. (a) A spin texture called skyrmion in chiral magnets (red to blue color denotes rotation of spin by π);[8,83] (b) magnetic monopoles (+ and – magnetic charges in a hexagonal configuration of nanomagnets) in artificial spin ice;[85] (c) double-core boojum structure in colloidal particles dispersed in a nematic liquid crystal. The correlation length ξ is related to the colloidal particle radius R = 0.1 μm ~ 9.3ξ. The color bars represent the degree of nematic biaxiality;[87] (d) Schlieren texture in a uniaxial nematic liquid crystal;[48,88,89] (e) multi-gon vortices in multiferroic thin films (different ferroelectric domain edges are denoted by red, blue, and green colors);[90] and (f) a pentagon-heptagon defect in a curved carbon nanotube (and inset shows the mitosis defect through a horizontal red line).[57]

https://doi.org/10.1557/mrs.2014.28 Published online by Cambridge University Press

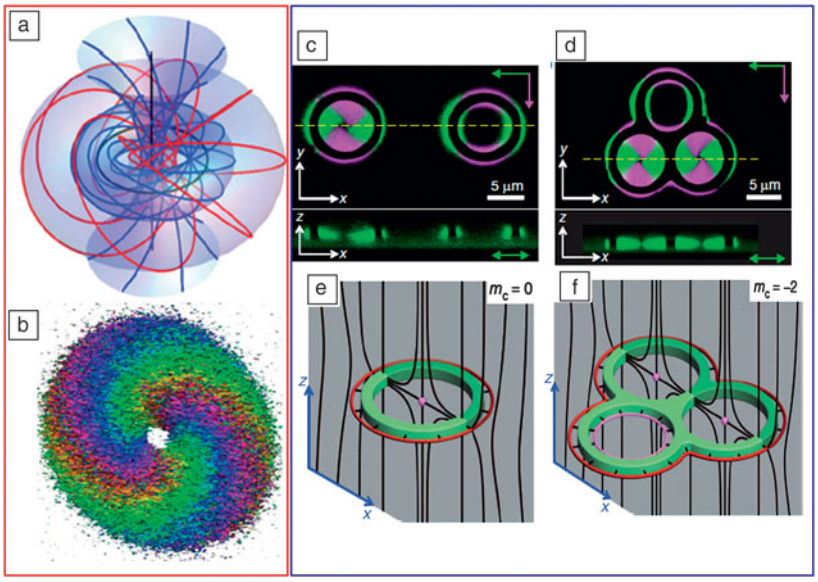


Figure 5. Illustration of topological metrology in two different experimental situations. (a) Schematic and (b) experimentally inferred image of an exotic topological defect called a Hopf fibration in a chiral nematic liquid crystal.[91] The image was obtained using three-photon excitation fluorescence polarizing microscopy (3PEF-PM) in conjunction with holographic optical tweezers. In the schematic, the flow lines with different colors correspond to different regions. In the image, winding bands of color meet at two hedgehog defects. The direction of the director field ranges from red to violet as the field rotates by π. (c) Single and (d) triple handlebody (g = 1,3, respectively) textures of non-spherical colloidal particles dispersed in a liquid crystal obtained by 3PEF-PM.[93] Green and magenta colors correspond to two orthogonal polarizations of excitation light. The cross-sectional image in the lower panels of (c) and (d) were obtained along the dashed yellow line. (e–f) Schematic diagrams of the corresponding director field (black lines). Red and magenta lines show outer and inner disclination loops.[93] In the (e) and (f) panels, m_c denotes the topological charge. (c–f) Adapted with permission from Reference 93.

defects, including the Hopf fibration. The latter was imaged[91] with three-photon excitation fluorescence polarizing microscopy in conjunction with holographic optical tweezers in the same optical setup. In fact, interfering light beams can create a textured molecular field in a liquid crystal, and optical laser lithography[92] can then be used to sculpt specific topological shapes out of a material. This approach opens up the exciting area of topological imaging in materials science.

Nonspherical colloidal particles with genus varying between 1 and 5 dispersed in nematic liquid crystals[93] underscore the importance of topology in materials science by way of inducing a zoo of topological defects and concomitant changes in material properties. These colloidal particles are accompanied by unusual topological defects with a net topological charge always equal to half of the Euler characteristic, $\chi/2$. Figure 5 exhibits results for g = 1, 3 as observed (Figure 5c–d), schematically indicating different configurations (Figure 5e–f). These experiments may enable topology-dictated elastic colloidal interactions and self-assembly of reconfigurable topological memory devices. Three-dimensional nonlinear optical imaging reveals that the topological charge is conserved. On the other hand, photothermal melting, laser tweezing, and electric fields cause transformations between these different configurations of colloidal particle-induced structures.

Some materials display topological disorder, which is quite distinct from the presence of topological defects. An example is that of 2D foams, where the distribution of the number of bubble sides provides a quantitative measure of topological disorder (as opposed to geometric disorder, which is related to the distribution of bubble area).[94] In particular, topological disorder in 2D foams (e.g., Table II) under shear can be measured by direct video imaging of a fluorescent tube, which provides bubble size-topology correlations.[94] For soft materials such as colloids, 3D nonlinear optical imaging is employed to measure the topological charge of defects. Similarly, external fields (electric, magnetic, pressure or stress), photothermal melting, laser tweezing, and other techniques are used to reveal their defect structures. Magnetic vortices and skyrmions are imaged via electron holography and Lorentz transmission electron microscopy. Schlieren imaging techniques could also come in handy when probing the topology of a variety of defects (e.g., in liquid crystals).[48,88] Next, we demonstrate how topology can be usefully invoked to determine the deformation energy of materials, specifically soft matter.

Elastic deformation energy

Biological vesicles have been observed to have a genus up to g = 3; however, synthetic vesicles can have very large values (~50) of g.[32] First, we start with the Helfrich-Canham curvature free energy:[33]

$$E_g = \int dS \; [\frac{\kappa_b}{2}(H - H_0)^2 + \kappa_G K], \qquad (2)$$

where κ_b= bending rigidity, κ_G= Gaussian rigidity, dS = element of surface, H_0 is the spontaneous mean curvature, and H and K are the mean and Gaussian curvature, respectively. Next, by using only topological means (such as Bogomol'nyi decomposition,[95] which is usually invoked to study topological invariance and indicates that the energy in Equation 2 is greater than or equal to $4\pi\,\kappa_G$ times a genus dependent term), one can calculate the elastic energy of deformation as a function of genus for vesicles,[95] as depicted in **Figure 6**. The energy increases monotonically with genus and asymptotically reaches the value of 8π, consistent with the Wilmore conjecture, a mathematical extrapolation.[95] From topological analysis, one finds that the spontaneous bending energy contribution resulting from any deformation of the vesicles from their metastable shapes falls into two distinct topological sets: shapes of spherical topology

https://doi.org/10.1557/mrs.2014.28 Published online by Cambridge University Press

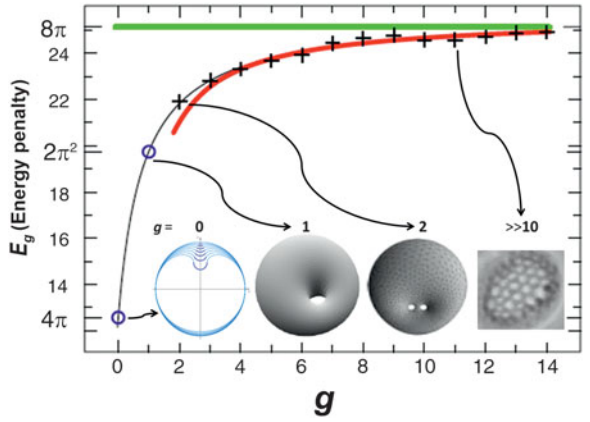


Figure 6. Elastic deformation energy of vesicles (E_g) as a function of genus (g).[95] Blue circles represent exact values; crosses represent numerical estimates computed with a (Brakke's) surface evolver. The red curve is an estimated fit to the deformation energy for large values of g. Green line denotes the asymptotic value of 8π.[95]

($g = 0$) and shapes of non-spherical topology ($g > 0$). These ideas can be readily applied to other materials and topologies.

Analogously, the deformation of negative curvature periodic minimal surfaces such as Schwarzites and double gyroids can be calculated, specifically under hydrostatic stress, assuming that only the lattice parameter changes under deformation.[20] Similarly, carbon and graphene nanoribbons can exist in helicoidal shape, and their axial deformation can be readily calculated by varying the pitch of the helicoid.[20] In both cases, the elastic energy is proportional to the Gaussian curvature and the material's bulk (or axial) modulus.

Finally, we consider topological quantum effects that are pervasive in condensed matter physics and have greatly enriched the discovery of novel phenomena as well as their attendant device applications.

Topological quantum effects

Topology is frequently invoked in condensed matter physics (wherein topology of the wave function affects the observed phenomena) such as in the quantum Hall effect;[1] the Aharonov–Bohm (AB) effect;[1] and many related effects[96,97] with applications in nanowire devices,[98] photonic waveguides,[99] and photonic quasicrystals.[100] Another quantum effect is the Casimir force that has found many applications in nanomechanics and nanoelectromechanical systems.[101] Furthermore, the topological Casimir effect has also been studied in CNTs, nanorings, and graphene.[102]

Topological materials and phase transitions

In materials such as topological insulators[4] (e.g., Bi_2Se_3, Bi_2Te_3) and topological superconductors[103] (e.g., $Cu_xBi_2Se_3$), the topological order changes under the influence of external fields, resulting in a topological phase transition. Topological order refers to a kind of order at zero temperature, which is macroscopically described as a "robust ground state degeneracy." It is also related to time reversal symmetry and spin-orbit coupling in materials, directly affecting the magnetoelectric response of the material. In topological insulators, the bulk is insulating, while the nontrivial topology of the bulk electronic energy bands demands that Dirac (i.e., relativistic) fermions are realized as surface states (which are metallic).[4] Instead of the usual quadratic dispersion, their electronic band structure has a linear dispersion (a Dirac cone) in the center of the band-gap that arises from the topological properties of their band structure. Analogously, topological crystalline insulators have been proposed as well.[104]

Dirac materials

Materials whose nontrivial electronic properties are a direct consequence of the linear energy Dirac spectrum $E_D = \nu k$, where E_D denotes the band electronic energy, ν is a constant, and k is the wave vector, are called "Dirac materials."[19,105,106] In other words, the conduction and valence bands touch at an isolated set of points called the Dirac points. Graphene, strong topological insulators[4] (Bi_2Se_3), and some d-wave superconductors[106,107] ($Bi_2Sr_2CaCu_2O_8$) are excellent examples. The motion of electrons in these materials is described not by the Schrödinger equation but by the Dirac equation. The low energy properties of Dirac materials are described by 2D massless Dirac fermions. These materials provide an entirely new avenue for exploring unusual electronic and thermal transport properties with potential applications. It is apparent that materials scientists are now primed to harness topological quantum effects in a slew of emerging topological materials.[18]

Summary and outlook

Using nanocarbons,[9,10] soft matter,[31,37,48] and biological systems[39,52] as illustrative examples, we have demonstrated that understanding the physical properties of a broad class of materials in terms of topology and geometry is not just useful but imperative for progress in materials science. We described the essential concepts of topology, topological characteristics, and their emerging role, clearly delineating the differences between local versus global topology, ubiquity, and importance of a menagerie of topological defects ranging from the commonplace domain walls to exotic skyrmions, boojums, and magnetic monopoles. Although topology is effectively elastic geometry, we emphasized the difference and how to link the two.

We also illustrated how RS, nonlinear optical imaging, and other analytical techniques adopted to topological characterization of materials provide a preliminary indication that a powerful topological metrology toolbox is now available to materials scientists. In particular, we identified the effects that arise due to curvature in lattice vibrational modes (usually ignored), and provided Raman spectra for otherwise unexplored nanoscale carbons in order to posit a truly viable topological metric.[9,10] This is a field in its infancy where many new metrological techniques are likely to be developed and discoveries are to be made in the near future.

https://doi.org/10.1557/mrs.2014.28 Published online by Cambridge University Press

In addition, we discussed complex and network topologies prevalent in soft matter, foams, DNA, proteins, and other biomaterials. We envision that novel topological and geometric characteristics can also be identified and adopted as metrics to design and synthesize advanced hard, soft, and biomacromolecular materials and analyze them from an entirely different perspective that explicitly incorporates topological metrology (i.e., a search for quantifying spatial and temporal topological correlations). Adopting theory, modeling, topological algorithms and databases,[16,17] and extensive simulation tools already used in condensed matter physics and quantum chemistry to the specific topological problems will accomplish these goals. As another manifestation of topology, using the Helfrich–Canham bending energy, we calculated the elastic deformation energy of vesicles with varying genus. Recent observations of multi-genus colloidal particles,[93] Hopf fibrations,[91] and dislocation reactions using topological tweezers[108] attest to the dawning of this field. Likewise, exploiting topological quantum effects and observing topological phase transitions is a significant growth area for research.[18] Consolidating metrology techniques for probing topology and redirecting geometric concepts toward topological applications are some of the new exciting frontiers, with a substantial scope for unanticipated discoveries. This combined approach of integrating modeling, design and synthesis, and metrology would undoubtedly usher in the powerful emergent paradigm of topology/geometry → property → functionality into materials science.

Acknowledgments

This work was supported in part by the US Department of Energy (A.S. and S.G. through LANL-CINT Gateway).

References

1. M. Nakahara, *Geometry, Topology and Physics, Graduate Student Series in Physics* (Taylor & Francis, Boca Raton, FL, 1990).
2. J.R. Munkres, *Topology*, *2nd ed.* (Pearson, London, 2000).
3. G.K. Francis, *A Topological Picturebook* (Springer, NY, 2006).
4. M. Hasan, C.L. Kane, *Rev. Mod. Phys.* **82**, 3045 (2010).
5. D. Massiot, R.J. Messinger, S. Cadars, M. Deschamps, V. Montouillout, N. Pellerin, E. Veron, M. Allix, P. Florian, F. Fayon, *Acc. Chem. Res.* **46**, 1975 (2013).
6. X. Zou, H. Ren, G. Zhu, *Chem. Commun.* **49**, 3911 (2013).
7. A.G. Evans, J.W. Hutchinson, N.A. Fleck, M.F. Ashby, H.N.G. Wadley, *Prog. Mater. Sci.* **46**, 309 (2001).
8. S. Muhlbauer, B. Binz, F. Jonietz, C. Pfleiderer, A. Rosch, A. Neubauer, R. Georgii, P. Boni, *Science* **323**, 915 (2009).
9. S. Gupta, A. Saxena, *J. Raman Spectrosc.* **39**, 1127 (2009).
10. S. Gupta, A. Saxena, *J. Appl. Phys.* **109**, 074316 (2011).
11. S.H. Yook, Z.N. Oltvai, A.L. Barabasi, *Proteomics* **4**, 928 (2004).
12. H. Yang, N. Coombs, G.A. Ozin, *Nature* **386**, 692 (1997).
13. D. Zhao, D.J. Timmons, D. Yuan, H.-C. Zhou, *Acc. Chem. Res.* **44**, 123 (2011).
14. N.J. Turro, M. Garcia-Garibay, in *Photochemistry in Organized and Constrained Media*, V. Ramamurthy, Ed. (VCH Publishers, New York, 1991), pp. 1–21.
15. S.T. Hyde, G.E. Schröder-Turk, *Interface Focus* **2**, 529 (2012).
16. http://www.topos.samsu.ru.
17. http://epinet.anu.edu.au/reference.
18. B. Yan, S.-C. Zhang, *Rep. Prog. Phys.* **75**, 096501 (2012).
19. J. Cayssol, *Condens. Matter* (2013), available at http://arxiv.org/abs/1310.0792.
20. S. Gupta, A. Saxena, *J. Appl. Phys.* **112**, 114316 (2012).
21. K.S. Novoselov, A.K. Geim, S.V. Morozov, D. Jiang, Y. Zhang, S.V. Dubonos, I.V. Grigorieva, A.A. Firsov, *Science* **306**, 666 (2004).
22. H. Kroto, J.R. Heath, S.C. O'Brien, R.E. Curl, R.E. Smalley, *Nature* **318**, 162 (1985).
23. A. Hirsch, M. Brettreich, *Fullerenes-Chemistry and Reactions* (Wiley, NY, 2004).
24. S. Tanda, T. Tsuneta, Y. Okajima, K. Inagaki, K. Yamaya, N. Hatakenaka, *Nature* **417**, 397 (2002).
25. A. Yamashiro, Y. Shimoi, K. Harigaya, K. Wakabayashi, *Physica E* **22**, 688 (2004).
26. J. Cai, P. Ruffieux, R. Jaafar, M. Bieri, T. Braun, S. Blankenburg, M. Matthias, A.P. Seitsonen, S. Moussa, X. Feng, K. Muellen, R. Fasel, *Nature* **466**, 470 (2010).
27. S.B. Sinnott, R. Andrews, *Crit. Rev. Solid State Mater. Sci.* **26**, 145 (2001).
28. A. Rubio, J. Corkill, M.L. Cohen, *Phys. Rev. B* **49**, 5081 (1994).
29. Y. Oshima, A. Onga, K. Takayanagi, *Phys. Rev. Lett.* **91**, 205503 (2003).
30. D. Ajami, O. Oeckler, A. Simon, R. Herges, *Nature* **426**, 819 (2003).
31. N. Hadjichristidis, S. Pispas, G. Floudas, *Block Copolymers: Synthetic Strategies, Physical Properties, and Applications* (Wiley, NY, 2003).
32. X. Michalet, D. Bensimon, *Science* **269**, 666 (1995).
33. R. Lipowsky, *Encyclopedia of Applied Physics* **23**, 199 (1998).
34. V. Saranathan, C.O. Osuji, S.G. Mochrie, H. Noh, S. Narayanan, A. Sandy, E.R. Dufresne, R.O. Prum, *Proc. Natl. Acad. Sci. U.S.A.* **107**, 11676 (2010).
35. E.J.W. Crossland, M. Kamperman, M. Nedelcu, C. Ducati, U. Wiesner, D.-M. Smilgies, G.E.S. Toombes, M.A. Hillmyer, S. Ludwigs, U. Steiner, H.J. Snaith *Nano Lett.* **9**, 2807 (2009).
36. R.B. King, *J. Chem. Inf. Comput. Sci.* **38**, 180 (1998).
37. S. Hutzler, D. Weaire, *The Physics of Foams* (Oxford University Press, UK, 1999).
38. S. Bohn, *Eur. Phys. J. E* **11**, 177 (2003).
39. A.T. Skjeltorp, *Knots and Applications to Biology, Chemistry and Physics* (Springer, NY, 1996).
40. B. Christensen, J. Nielsen, *Adv. Biochem. Eng. Biotechnol.* **66**, 209 (2000).
41. L.H. Sperling, *J. Polym. Sci. Macromol. Rev.* **12**, 141 (1977).
42. E.A. Lazar, J.K. Mason, R.D. MacPherson, D.J. Srolovitz, *Phys. Rev. Lett.* **109**, 095505 (2012).
43. X. Huang, A. Radman, Y.M. Xie, *Comput. Mater. Sci.* **50**, 1861 (2011).
44. L.W. Hobbs, C.E. Jesurum, V. Pulim, B. Berger, *Philos. Mag. A* **78**, 679 (1998).
45. T. Ishøy, K. Mortensen, *Langmuir* **21**, 1766 (2005).
46. R.D. Hills Jr., S.V. Kathuria, L.A. Wallace, I.J. Day, C.L. Brooks 3rd, C.R. Matthews, *J. Mol. Biol.* **398**, 332 (2010).
47. W.L. Wang, O.V. Yazyev, S. Meng, E. Kaxiras, *Phys. Rev. Lett.* **102**, 157201 (2009).
48. O.D. Lavrentovich, in *Patterns of Symmetry Breaking*, H. Arodz, J. Dziarmaga, W.H. Zurek, Eds. (Kluwer Academic, The Netherlands, 2003), pp. 161–195.
49. E.A. Matsumoto, G.P. Alexander, R.D. Kamien, *Phys. Rev. Lett.* **103**, 257804 (2009).
50. A.H. Schoen, NASA Technical Note TN D-5541 (1970).
51. E. Sezgin, H.-J. Kaiser, T. Baumgart, P. Schwille, K. Simons, I. Levental, *Nat. Protoc.* **7**, 1042 (2012).
52. J. Katsaras, T. Gutberlet, Eds., in *Lipid Bilayers – Structure and Interactions* (Springer-Verlag, Berlin-Heidelberg, 2001).
53. M.A. Pimenta, G. Dresselhaus, M.S. Dresselhaus, L.G. Cancádo, A. Jorio, R. Saito, *Phys. Chem. Chem. Phys.* **9**, 1276 (2007), and references therein.
54. M.S. Dresselhaus, P.C. Eklund, *Adv. Phys.* **49**, 705 (2000).
55. J.-C. Charlier, *Acc. Chem. Res.* **35**, 1063 (2002).
56. S. Iijima, T. Ichihashi, Y. Ando, *Nature* **356**, 776 (1992).
57. L. Chico, V.H. Crespi, L.X. Benedict, S.G. Louie, M.L. Cohen, *Phys. Rev. Lett.* **76**, 971 (1996).
58. J.K. Pachos, *Contemp. Phys.* **50**, 375 (2009).
59. I. Zsoldos, *J. Nanotechnol. Sci. Appl.* **3**, 101 (2010).
60. E.J. Duplock, M. Scheffler, P.J.D. Lindan, *Phys. Rev. Lett.* **92**, 225502 (2004).
61. S. Gupta, R.J. Patel, *J. Raman Spectrosc.* **38**, 188 (2007).
62. V.N. Mochalin, O. Shenderova, D. Ho, Y. Gogotsi, *Nat. Nanotechnol.* **7**, 11 (2011).
63. X. Blasé, L.X. Benedict, E.L. Shirley, S.G. Louie, *Phys. Rev. Lett.* **72**, 1878 (1994).
64. A.C. Ferrari, D.M. Basko, *Nat. Nanotechnol.* **8**, 235 (2013).
65. L. Dunsch, F. Ziegs, J. Fröhner, U. Kirbach, K. Klostermann, A. Bartl, U. Feist, *Electronic Properties of Fullerenes, Springer Series in Solid-State Sciences* (Springer, NY, 1993), vol. 117, pp. 39–43.
66. E. Yamamoto, M. Tansho, T. Tomiyama, H. Shinohara, H. Kawahara, Y. Kobayashi, *Am. Chem. Soc.* **118**, 2293 (1996).
67. M. Takata, E. Nishibori, B. Umeda, M. Sakata, E. Yamamoto, H. Shinohara, *Phys. Rev. Lett.* **78**, 3330 (1997).
68. H. Wang, M. Chhowalla, N. Sano, S. Jia, G.A.J. Amaratunga, *Nanotechnology* **15**, 546 (2004).

https://doi.org/10.1557/mrs.2014.28 Published online by Cambridge University Press

69. K. Murata, J. Miyawaki, M. Yudasaka, S. Iijima, K. Kaneko, *Carbon* **43**, 2826 (2005).
70. M. Yudasaka, T. Komatsu, T. Ichihashi, Y. Achiba, S. Iijima, *J. Phys. Chem. B* **107**, 4681(2003).
71. P. Tan, S. Dimovski, Y. Gogotsi, *Philos. Trans. R. Soc. London, A* **362**, 2289 (2004).
72. V. Meunier, Ph. Lambin, A.A. Lucas, *Phys. Rev. B* **57**, 14886 (1998).
73. J.C. Charlier, G.M. Rignanese, *Phys. Rev. Lett.* **86**, 5970 (2001).
74. R.P. Vidano, D.B. Fishbach, L.J. Willis, T.M. Loehr, *Solid State Commun.* **39**, 341 (1981).
75. A.V. Baranov, A.N. Bekhterev, Y.S. Bobovich, V.I. Petrov, *Opt. Spectrosc.* **62**, 1036 (1987).
76. C. Thomsen, S. Reich, *Phys. Rev. Lett.* **85**, 5214 (2000).
77. V. Mennella, G. Monaco, L. Colangeli, E. Bussoletti, *Carbon* **33**, 115 (1995).
78. H.-J. Vogel, *Lecture Notes in Physics*, K.R. Mecke, D. Stoyan, Eds. (Springer-Verlag, Berlin, 2002), vol. 600, pp. 75–92.
79. H.K. Chae, D.Y. Siberio-Perez, J. Kim, Y.-B. Go, M. Eddaoudi, A.J. Matzger, M. O'Keefe, O.M. Yaghi, *Nature* **427**, 523 (2004).
80. G.-H. Lee, R.C. Cooper, S.J. An, S. Lee, A. van der Zande, N. Petrone, A.G. Hammerberg, C. Lee, B. Crawford, W. Oliver, J.W. Kysar, J. Hone, *Science* **340**, 1073 (2013).
81. R. Gröger, T. Lookman, A. Saxena, *Phys. Rev. B* **78**, 184101 (2008).
82. T. Dauxois, M. Peyrard, *Physics of Solitons* (Cambridge University Press, UK, 2006).
83. S. Seki, X.Z. Yu, S. Ishiwata, Y. Tokura, *Science* **336**, 198 (2012).
84. J. Fukuda, S. Zumer, *Nat. Commun.* **2**, 246 (2011).
85. S. Zhang, I. Gilbert, C. Nisoli, G.-W. Chern, M.J. Erickson, L. O'Brien, C. Leighton, P.E. Lammert, V.H. Crespi, P. Schiffer, *Nature* **500**, 553 (2013).
86. P. Milde, D. Kohler, J. Seidel, L.M. Eng, A. Bauer, A. Chacon, J. Kindervater, S. Muhlbauer, C. Pfleiderer, S. Buhrandt, C. Schutte, A. Rosch, *Science* **340**, 1076 (2013).
87. M. Tasinkevych, N.M. Silvestre, M.M. Telo da Gama, *New J. Phys.* **14**, 073030 (2012).
88. G.S. Settles, *Schlieren and Shadowgraph Techniques: Visualizing Phenomena in Transparent Media* (Springer-Verlag, Berlin, 2001).
89. I. Dierking, O. Marshall, J. Wright, N. Bulleid, *Phys. Rev. E* **71**, 061709 (2005).
90. S.C. Chae, Y. Horibe, D.Y. Jeong, S. Rodan, N. Lee, S.W. Cheong, *Proc. Natl. Acad. Sci. U.S.A.* **107**, 21366 (2010).
91. B.G. Chen, P.J. Ackerman, G.P. Alexander, R.D. Kamien, I.I. Smalyukh, *Phys. Rev. Lett.* **110**, 237801 (2013).
92. J. Fischer, M. Wegener, *Laser Photonics Rev.* **7**, 22 (2013).
93. B. Senyuk, Q. Liu, S. He, R.D. Kamien, R.B. Kusner, T.C. Lubensky, I.I. Smalyukh, *Nature* **493**, 200 (2013).
94. C. Quillet, S.A. Talebi, D. Rabaud, J. Kafer, S.J. Cox, F. Graner, *Philos. Mag. Lett.* **88**, 651 (2008).
95. J. Benoit, A. Saxena, T. Lookman, *J. Phys. A* **34**, 9417 (2001).
96. Y. Aharonov, A. Casher, *Phys. Rev. Lett.* **53**, 319 (1984).
97. Y. Aharonov, J. Anandan, *Phys. Rev. Lett.* **58**, 1593 (1987).
98. V. Mourik, K. Zuo, S.M. Frolov, S.R. Plissard, E.P.A.M. Bakkers, L.P. Kouwenhoven, *Science* **336**, 1003 (2012).
99. F.D.M. Haldane, S. Raghu, *Phys. Rev. Lett.* **100**, 013904 (2008).
100. M. Verbin, O. Zilberberg, Y.E. Kraus, Y. Lahini, Y. Silberberg, *Phys. Rev. Lett.* **110**, 076403 (2013).
101. V.M. Mostepanenko, N.N. Trunov, *The Casimir Effect and Its Applications* (Clarendon, Oxford, 1997).
102. S. Bellucci, A.A. Saharian, *Phys. Rev. D* **80**, 105003 (2009).
103. S. Sasaki, M. Kriener, K. Segawa, K. Yada, Y. Tanaka, M. Sato, Y. Ando, *Phys. Rev. Lett.* **107**, 217001 (2011).
104. L. Fu, *Phys. Rev. Lett.* **106**, 106802 (2011).
105. E. Rossi, J.H. Bardarson, M.S. Fuhrer, S. Das Sarma, *Phys. Rev. Lett.* **109**, 096801 (2012).
106. A.V. Balatsky, I. Vekhter, J.-X. Zhu, *Rev. Mod. Phys.* **78**, 373 (2006).
107. T.O. Wehling, A.M. Black-Schaffer, A.V. Balatsky, *Adv. Phys.*, in press (2014).
108. W.T.M. Irvine, A.D. Hollingsworth, D.G. Grier, P.M. Chaikin, *Proc. Nat. Acad. Sci. U.S.A.* **110**, 15544 (2013). □



Sanju Gupta has been an associate professor of physics at Western Kentucky University since August 2013. She holds an adjunct professor position at Drexel University, Philadelphia. Her main research interests are experimental condensed-matter materials physics and biophysics. She is a recipient of NIH, NSF, and JSPS fellowships. Gupta also is a member of the Materials Research Society, the American Physical Society, American NanoSociety, and the American Vacuum Society. Gupta can be reached at the Department of Physics and Astronomy, Western Kentucky University, USA; tel. 270-745-5940; and email sanju.gupta@wku.edu.



Avadh Saxena is a group leader of the Physics of Condensed Matter and Complex Systems group at Los Alamos National Laboratory, where he has been since 1990. He holds adjunct professor positions at the University of Barcelona, Spain, and the University of Arizona, Tucson. He also is a scientific advisor to the National Institute for Materials Science (NIMS), Tsukuba, Japan, and the Institute for Nanoscience and Nanotechnology at the University of Barcelona. Saxena's main research interests include phase transitions, optical, electronic, magnetic, transport, and vibrational properties of functional materials. He is a member of the American Physical Society, the Materials Research Society, and the Sigma Xi Scientific Research Society. Saxena can be reached at the Los Alamos National Laboratory, Los Alamos, NM, USA; tel. 505-667-5227; and email avadh@lanl.gov.

Career Center

JOB SEEKERS MEET YOUR NEXT EMPLOYER!

We'll show off your talents to the world's most prestigious high-tech firms, universities and laboratories. At the 2014 MRS Spring Meeting Career Center, you can access many interesting job postings, visit recruitment booths and interview with prospective employers. Please bring extra copies of your resume for your own use.

The Career Center is FREE to all MRS members and those registered to attend the 2014 MRS Spring Meeting.

ON-SITE REGISTRATION HOURS
Monday, April 21.....1:00 pm – 4:00 pm
(Candidate Registration Only)

CAREER CENTER HOURS
Tuesday, April 22 .....10:00 am – 5:00 pm
Wednesday, April 23.....10:00 am – 5:00 pm

Register and submit your resume today!
www.mrs.org/spring-2014-career-center



https://doi.org/10.1557/mrs.2014.28 Published online by Cambridge University Press

Materials Research Society®

University Chapters

The Materials Research Society® (MRS) University Chapter Program is a passionate and talented network of students from universities around the world. Supported by the Materials Research Society Foundation, the program fosters an environment for collaboration and open exchange of ideas across all scientific disciplines, spanning campuses and continents. These students represent the next generation of materials research and are preparing to carry the torch forward, advancing materials and improving the quality of life.

You'll find starting an MRS University Chapter is a fun and exceptionally valuable experience. Working through your Chapter—hosting events, creating special projects and connecting with experts from around the world—will prepare you for future professional and leadership roles in the materials community. Your Chapter can also play a vital role in bringing science to a broader audience. Now more than ever, the goal is to successfully bring research out of the laboratory and into the classroom and to the general public … to show how materials have changed our history and continue to shape our future.

MRS continues to explore new ways to effectively foster growth of virtual global materials communities, using emerging technologies that are smart, fresh and innovative … and that includes our University Chapters. With social media, MRS OnDemand® and two-way live streaming, we're already tapping into today's technologies to engage Chapters unable to attend our Meetings, but with the promise of new innovations, tools and devices, we continue to look ahead. **Help us build the Chapter of the Future!** Together we can design and develop virtual events to better collaborate, educate, participate and fascinate—across Chapters, across disciplines, across borders.

Now's the time to use your excitement, expertise and unique scientific perspectives to forge a new path. Join this international student community.

Start an MRS University Chapter today!

MATERIALS RESEARCH SOCIETY FOUNDATION

HELP US BUILD THE FUTURE

An International Community

One of the main objectives as graduate students and future researchers is to acquire the ability to build scientific networks for enhancing our vision, mission and scientific cooperation. MRS offers multiple tools to accomplish this with annual meetings, workshops, the MRS Bulletin and useful applications such as career connections or MRS OnDemand. Our MRS Student Chapter allowed us to obtain support from the Sociedad Mexicana de Materiales (SMM) that expands our national network. The formation of MRS Cinvestav Student Chapter not only allows us to integrate and exchange ideas as materials science students at Cinvestav, but also have the opportunity to know the science beyond our borders.

Natalia Tapia, Chapter President
Centro de Investigación y de Estudios Avanzados
del Instituto Politécnico Nacional (Cinvestav-IPN)
Mexico City, MEXICO

Interdisciplinary Collaboration

The MRS Student Chapter at WSU was organized by students who recognized the need to bring together a diverse group of students who were working in materials science. The campus is spread out geographically and students pursuing PhD degrees in MSE can be advised by chemistry or physics professors who are located far from the MSE department located in the engineering buildings. There is no distinction made between students whose advisors are in different departments or colleges, and the MRS Student Chapter has been a great vehicle to promote unity within the disciplines here.

David Field, Chapter Faculty Advisor
Washington State University
Pullman, Washington, USA

https://doi.org/10.1557/mrs.2014.28 Published online by Cambridge University Press

The MRS University Chapter Experience

The MRS University Chapter Program provides invaluable experiences and benefits for student members, but don't take our word for it. **Our Chapter Members Say It Best!**

Leadership Development

The Materials Research Society, along with our local Binghamton University Chapter, has positively influenced my commitment to materials science and technology. We were inspired by our advisor, Professor M. Stanley Whittingham, to start this Chapter … and motivated by his enthusiasm and our faith to bring science to the general public, we continue to hold numerous events taken from MRS, i.e. MAKING STUFF and NanoDays. As our organization grows, we keep growing our events, and have found a solid and welcoming place in our community. Apart from the target audience, our events also benefit the volunteers, who gained valuable experience both from preparation, interaction, and activities. We feel proud and grateful to be part of an MRS University Chapter.

Tianchan Jiang, Chapter President
Binghamton University
Binghamton, New York, USA

Education Outreach

Our Chapter has enabled us to establish collaborations among the scientists on campus through informal social events, in addition to providing opportunities to participate in outreach. Integrating the science outreach efforts of Vanderbilt's community into our local community is one of our primary goals. As a University Chapter, we received a grant through the Materials Research Society Foundation to bring emerging materials science and hands-on activities to disadvantaged students and teachers in rural Tennessee. Without these seed funds, our Vanderbilt program, Materials Outreach for Rural Education (MORE), would not have been possible.

Amy Ng, Chapter President
Vanderbilt/Fisk Universities
Nashville, Tennessee, USA

Professional Growth

Starting and advising an MRS University Chapter is truly a rewarding experience. One can see professional growth of students, who start feeling like members of the worldwide materials research community. I come to MRS meetings with a "team," not just a couple of my students. Exciting initiatives and project ideas generated by students are amazing. Not surprisingly, some of the most prominent materials scientists, such as Millie Dresselhaus (MIT) or Stan Whittingham (SUNY Binghamton), have been acting as Faculty Advisors for many years.

Yury Gogotsi, Chapter Faculty Advisor
Drexel University
Philadelphia, Pennsylvania, USA

Building Chapters of the Future

I had the chance to present at the 2012 MRS Fall Meeting's Sustainability Forum, while being over 9000 km away from the meeting venue. I felt as if I was actually in Boston, being able to take questions, address them and getting into discussions with the committee. Thanks to the Materials Research Society and our local MRS-KAUST University Chapter for making this possible.

Ahmed E. Mansour, Chapter Vice President
King Abdullah University of Science and Technology (KAUST)
Thuwal, SAUDI ARABIA

Chapter Support

As a graduate student, it is key to broaden your spectrum of what is taking place in the research world in real time. MRS opens up many avenues, especially when working from a University Chapter. Direct contact with MRS associates helps keep everyone abreast of conferences, Chapter opportunities and activities that otherwise may not have been as easily accessible. MRS also rewards student memberships with rebates and travel expenditures, helping promote student involvement as well as Chapter building. We were able to host a multitude of meetings and seminars as well as send students to attend MRS conferences to promote their research.

Chinedu Okoro, Chapter President
Tuskegee University
Tuskegee, Alabama, USA

FOR MORE INFORMATION

on the MRS University Chapter Program,
visit **www.mrs.org/university-chapters**

https://doi.org/10.1557/mrs.2014.28 Published online by Cambridge University Press